

## Impact of phase lag on synchronization in frustrated Kuramoto model with higher-order interactions

Sangita Dutta,<sup>1,\*</sup> Abhijit Mondal,<sup>1</sup> Prosenjit Kundu,<sup>2,†</sup> Pitambar Khanra,<sup>3,‡</sup> Pinaki Pal,<sup>1,§</sup> and Chittaranjan Hens<sup>4</sup>

<sup>1</sup>*Department of Mathematics, National Institute of Technology, Durgapur 713209, India*

<sup>2</sup>*Dhirubhai Ambani Institute of Information and Communication Technology, Gandhinagar, Gujarat 382007, India*

<sup>3</sup>*Department of Mathematics, State University of New York at Buffalo, Buffalo 14260, USA*

<sup>4</sup>*Center for Computational Natural Science and Bioinformatics, International Institute of Informational Technology, Gachibowli, Hyderabad 500032, India*



(Received 4 May 2023; accepted 25 August 2023; published 18 September 2023)

The study of first order transition (explosive synchronization) in an ensemble (network) of coupled oscillators has been the topic of paramount interest among the researchers for more than one decade. Several frameworks have been proposed to induce explosive synchronization in a network and it has been reported that phase frustration in a network usually suppresses first order transition in the presence of pairwise interactions among the oscillators. However, on the contrary, by considering networks of phase frustrated coupled oscillators in the presence of higher-order interactions (up to 2-simplexes) we show here, under certain conditions, phase frustration can promote explosive synchronization in a network. A low-dimensional model of the network in the thermodynamic limit is derived using the Ott-Antonsen ansatz to explain this surprising result. Analytical treatment of the low-dimensional model, including bifurcation analysis, explains the apparent counter intuitive result quite clearly.

DOI: [10.1103/PhysRevE.108.034208](https://doi.org/10.1103/PhysRevE.108.034208)

### I. INTRODUCTION

Synchronization [1–3] is a captivating phenomenon observed in natural and artificial systems [4–14]. A large set of coupled oscillators undergoes a continuous synchronization transition if the interaction strength among themselves is gradually increased. To describe such transition, a simple and analytically tractable phase model was developed by Yoshiki Kuramoto [10], in which each oscillator has its own intrinsic frequency ( $\omega_i$ ), and cross-talks to each other via a periodic coupling function representing pairwise interactions. The phase of the  $i$ th oscillator is given by

$$\dot{\theta}_i = \omega_i + K \sum_{j=1}^N \sin(\theta_j - \theta_i), \quad i = 1, 2, \dots, N, \quad (1)$$

where  $K$  is the coupling strength and  $\theta_i$  is the phase of the  $i$ th oscillator. To measure the level of synchronization, the order parameter  $r$  is defined as

$$r e^{i\psi} = \frac{1}{N} \sum_{j=1}^N e^{i\theta_j}. \quad (2)$$

The classical Kuramoto model (KM) [10,15] described above shows second order (continuous) or first order (explosive)

transition to synchronization ( $r \rightarrow 1$ ) state depending on the choice of natural frequencies, as the coupling strength is gradually increased from a small value. In general, it shows second order transition for unimodal frequency distributions [2], whereas first order transition is observed for uniform or bimodal distribution of frequencies [16,17,19]. All the oscillators rotate with the mean of the natural frequencies in a higher coupling strength. However, different scenarios may appear if a phase-lag or frustration parameter ( $\beta$ ) [13,18–27] is introduced in the pairwise coupling function [ $\sin(\theta_j - \theta_i - \beta)$ ]. This phase-lag parameter shifts the system's synchronous frequency from the mean natural frequency. Thus,  $\beta$  can be used as a control parameter that can tune the mean frequency to a desired one [24]. The model was first introduced by Sakaguchi jointly with Kuramoto and is presently known as the Sakaguchi-Kuramoto (SK) model. In the SK model, the phase lag  $\beta$  generally opposes the coupled system to reach to the global synchronous state and consequently, higher coupling strength compared to KM is required for achieving a desired level of synchronization. Also, for a particular choice of frequencies, the synchronization may deviate from the universal continuous transition route [19,28,29]. Further it has been shown, that in a complex network setup, the SK model cannot reach a global synchronous state (called erosion of synchronization) [30]. Even over a critical  $\beta$ , where the natural frequencies are correlated with degree, the hysteresis or explosive width can entirely vanish, and the level of synchronization would be significantly reduced [20]. To overcome such situations, the design of suitable frequencies [22,23,31], usage of multiple layers of networks [32–34], and time-dependent coupling functions [35] have been proposed.

\* sangitaduttaprl@gmail.com

† jitprosen.math@gmail.com

‡ pitambar.khanra89@gmail.com

§ pinaki.pal@maths.nitdgp.ac.in

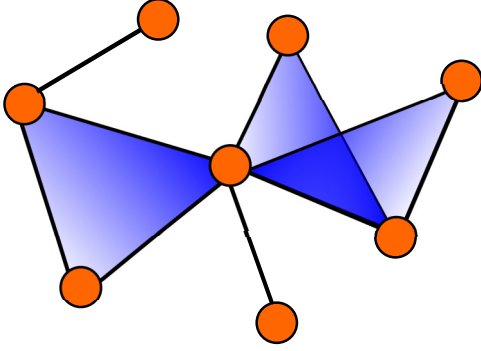


FIG. 1. Schematic diagram of a simplicial complex consisting of 0-simplex (circles), 1-simplex (edges), and 2-simplex (triangles).

Note that models of Josephson junction arrays [13], power network systems [27], dynamics of mechanical rotors [36], quantum networks [26] all can be captured by such phase-lag oscillators under the paradigm of pairwise interactions.

However, in recent studies the importance of incorporating higher-order interactions (HOI) along with its pairwise counterpart has been emphasized [37–50]. Specifically, the works on neuroscience [45–47,51], ecology [52–55] and physics [56] have highlighted the crucial role of such higher-order interactions (e.g., in a collaboration network multiauthor collaboration [57]) in addition to pairwise one. Simplicial complexes [58,59] can successfully encode these higher-order structures. An  $n$  simplex is formed by  $(n + 1)$  interacting units, consisting of all the  $d$  ( $< n$ ) simplexes. For example, 1-simplex denotes the pairwise interactions, 2-simplex denotes the three way interactions, including pairwise one, and so on. These simplices adhere to one another along their sides, and form a simplicial complex. Figure 1 represents a schematic diagram of a simplicial complex with higher-order interactions. Until now some of the dynamical behaviors induced by the HOI have been explored including multistability [60,61], chimera states [62], chaos [63], etc. Also, it has been shown that the presence of HOI along with pairwise interactions can produce high levels of synchronization in weaker coupling strength [64] and may lead to the first order or discontinuous transition to desynchronization [60]. Recently, Skardal *et al.* has reported in [65] that the HOI in a simplicial complex can exhibit abrupt transition to synchrony, without any degree frequency correlation. Subsequently, in [66], it has been demonstrated that adaptation to higher-order coupling leads to tired synchronization transition in addition to second order transition.

In this paper, we consider the SK model with HOI under the all-to-all coupling configuration and observe a significantly different effect of phase frustration compared to the ones observed in the presence of solely pairwise interactions. For simplicity we restrict ourselves toward pairwise and triadic interactions only. It is observed that instead of inhibiting discontinuous transition to synchronization, phase-lag promotes it in certain regions of the parameter space in the presence of HOI. This surprising result is explained based on an analytical framework based on Ott-Antonsen ansatz [67].

## II. MODEL DESCRIPTION AND NUMERICAL SIMULATIONS

The dynamics of a phase frustrated undirected simplicial complex of  $N$  number of nodes with global connectivity is governed by the following system of equations:

$$\begin{aligned} \dot{\theta}_i = & \omega_i + \frac{K_1}{N} \sum_{j=1}^N \sin(\theta_j - \theta_i - \beta) \\ & + \frac{K_2}{N^2} \sum_{j=1}^N \sum_{l=1}^N \sin(2\theta_j - \theta_l - \theta_i - \beta), \\ & i = 1, 2, \dots, N. \end{aligned} \quad (3)$$

This is the generalization of the classical Sakaguchi-Kuramoto model obtained by incorporating HOI along with pairwise ones. Here  $\theta_i$  represents the phase and  $\omega_i$  is the natural frequency of the  $i$ th oscillator, and  $\omega$  is drawn from a Lorentzian distribution with density function  $g(\omega) = \frac{\Delta}{\pi[\Delta^2 + (\omega - \omega_0)^2]}$  with mean  $\omega_0$ .  $\beta$  denotes the uniform phase-lag of the system.  $K_1$  and  $K_2$  are the coupling strengths of pairwise interactions and HOI, respectively. Two complex order parameters associated with 1-simplex and 2-simplex are defined by

$$z = r e^{i\psi} = \frac{1}{N} \sum_{j=1}^N e^{i\theta_j}, \quad z_2 = r_2 e^{i\psi_2} = \frac{1}{N} \sum_{j=1}^N e^{2i\theta_j}, \quad (4)$$

where the amplitudes  $r = |z|$  and  $r_2 = |z_2|$  of the order parameters  $z$  and  $z_2$ , respectively, measures the level of synchronization, and  $\psi$  and  $\psi_2$  are the respective arguments, representing the average phases of the oscillators.

To find the effect of the phase frustration on the SK model with HOI, we simulate the equations (3) with network size  $N = 10^3$  by the fourth order Runge-Kutta method with time step  $\delta t = 0.01$ . First we set  $K_2 = 8$  and check the effect of  $\beta$  by varying it in the range of  $[0, \frac{\pi}{2})$ . Initially, the phases of the oscillators are spread uniformly at random around a circle. The natural frequencies are drawn from a Lorentzian distribution with mean 0 and half width  $\Delta = 1$ . To determine the nature of transitions to synchronization we continue the simulation of the system (3) by varying the relevant parameter both in forward and backward directions. For forward continuation, the simulation is started with  $K_1 = -1$  and continued until  $K_1 = 12$  by increasing it in small steps to achieve the synchronized state and for backward continuation, simulation is started with  $K_1 = 12$  and continued until  $K_1 = -1$  by gradually decreasing  $K_1$  in small steps. Note that, during forward and backward continuation, the final state of the previous simulation is taken as the initial condition for the present simulation. Figure 2(a) shows the variation of  $r$  with  $K_1$  for different values of  $\beta$ , namely,  $\beta = 0$  (blue),  $\beta = 1$  (magenta),  $\beta = 1.2$  (cyan),  $\beta = 1.318$  (green), and  $\beta = 1.35$  (red) for both forward and backward continuations. It is seen that the system exhibits discontinuous synchronization transition for smaller  $\beta$  and it becomes continuous as  $\beta$  is gradually increased. Also, it is evident from Fig. 2(a) that the hysteresis width for the synchronization transition decreases with the increase of  $\beta$  and the transition becomes continuous for  $\beta > 1.318$ .

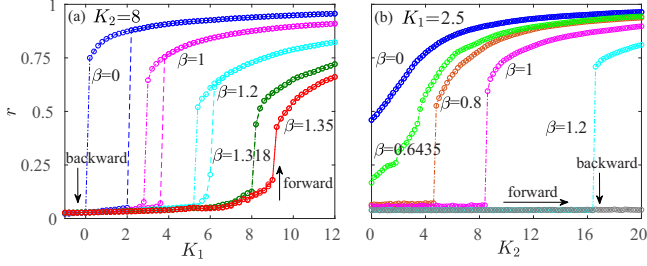


FIG. 2. Numerically obtained synchronization profile of the global network for different phase-lag values. Forward and backward transitions are indicated by up and down arrows, respectively. (a)  $r$  is shown as a function of  $K_1$  for fixed  $K_2 = 8$ . (b) For fixed  $K_1 = 2.5$ ,  $r$  is plotted as a function of  $K_2$  for various  $\beta$ .

Next, to understand the impact of HOI coupling strength  $K_2$  on the synchronization transition, we simulate the system (3) by varying  $K_2$  with fixed  $K_1 = 2.5$  for different  $\beta$ . The variation of the order parameter  $r$  with respect to  $K_2$  is presented in Fig. 2(b). It is observed that for a low  $\beta$  value [ $\beta = 0$  (blue) and 0.6435 (bright green)],  $r$  follows a continuous transition. On the other hand, for  $\beta > 0.6435$ , say for  $\beta = 0.8$  (brown), 1 (magenta), and 1.2 (cyan), discontinuous transitions to synchronization are observed. Therefore, it is clearly observed that with the increase of  $\beta$  the backward transition points move forward but discontinuous transition is not suppressed by higher  $\beta$ . This surprising result seems to be a unique feature of HOI. Here the effect is opposite to the one that is observed in presence of pairwise interactions only, where phase frustration is known to suppress the discontinuous transition to synchronization [20]. To develop a deeper understanding about this interesting result we proceed to derive a low-dimensional model (LDM) of the system (3) using Ott-Antonsen ansatz [67].

### III. A LOW-DIMENSIONAL MODEL

In this section we derive a (LDM) to explain the numerically observed transition to synchronization in the system. First we write the equation (3) with the help of the equation (4) as

$$\dot{\theta}_i = \omega_i + \frac{1}{2i} [e^{-i(\theta_i + \beta)} H - e^{i(\theta_i + \beta)} \bar{H}], \quad (5)$$

where  $H = K_1 z + K_2 z_2 \bar{z}$  and the overbar denotes complex conjugate. In the thermodynamic limit, we assume that the density of the oscillators with phase  $\theta$ , frequency  $\omega$  at time  $t$  is given by  $f(\theta, \omega, t)$ . Since the natural frequency is drawn from a distribution  $g(\omega)$ , the function  $f$  can be expanded in a Fourier series as

$$f = \frac{g(\omega)}{2\pi} \left[ 1 + \sum_{n=1}^{\infty} [f_n(\omega, t) e^{in\theta} + c.c.] \right], \quad (6)$$

where  $c.c.$  denotes the complex conjugate and  $f_n(\omega, t)$  is the coefficient of the  $n$ th term of the series. Now, following the Ott-Antonsen ansatz [67], we take  $f_n = \alpha^n$  for some analytic function  $\alpha$ . The conservation of the oscillators in the network

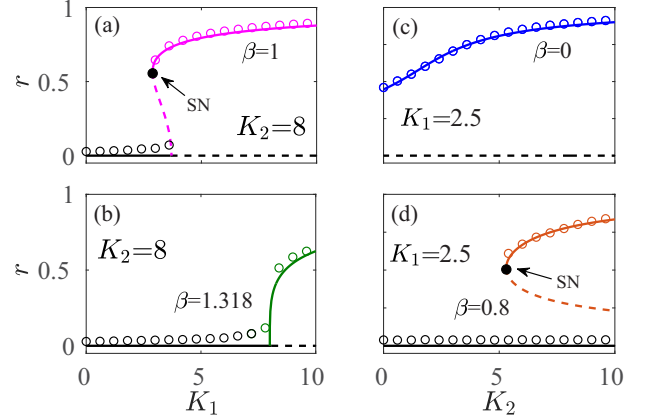


FIG. 3. Bifurcation diagrams prepared using the LDM. First column [(a)-(b)]:  $r$  as a function of  $K_1$  for  $K_2 = 8$  with  $\beta = 1$  and 1.318; Second column [(c)-(d)]: the variation of  $r$  with  $K_2$  for  $K_1 = 2.5$  with  $\beta = 0$  and 0.8 respectively. Solid and dashed lines are obtained from the LDM, and respectively represent the stable and unstable equilibria. The filled black circles show the saddle-node (SN) bifurcation points. The colored circles show the values of  $r$  corresponding to the stable solutions as obtained in the numerical simulation.

leads to the following continuity equation

$$\frac{\partial f}{\partial t} + \frac{\partial}{\partial \theta} (fv) = 0, \quad (7)$$

where  $v = \frac{d\theta}{dt}$  is the velocity given by Eq. (5). Replacing  $f$  by its Fourier series representation (6) in the continuity equation, we obtain

$$\dot{\alpha} + i\alpha\omega + \frac{1}{2} [H\alpha^2 e^{-i\beta} - \bar{H}e^{i\beta}] = 0. \quad (8)$$

Integrating the complex order parameter in the lower half of the complex plane using the Cauchy's integral theorem we get,  $\bar{z} = \alpha(\omega_0 - i\Delta, t)$ . Similarly, we can derive  $\bar{z}_2 = \alpha^2(\omega_0 - i\Delta, t) = \bar{z}^2$ . At  $\omega = \omega_0 - i\Delta$ , Eq. (8) leads to

$$\dot{z} = iz\omega_0 - z\Delta + \frac{1}{2} [(K_1 z + K_2 z^2 \bar{z}) e^{-i\beta} - z^2 (K_1 \bar{z} + K_2 \bar{z}^2 z) e^{i\beta}]. \quad (9)$$

Putting  $z = re^{i\psi}$  and comparing real and imaginary parts on both sides of Eq. (9), we obtain the following LDM for the system (3):

$$\dot{r} = -\Delta r + \frac{\cos \beta}{2} (K_1 r + K_2 r^3) [1 - r^2], \quad (10)$$

$$\dot{\psi} = \omega_0 - \frac{\sin \beta}{2} (K_1 + K_2 r^2) [1 + r^2]. \quad (11)$$

The LDM is now used for analytical treatment in the following section.

### IV. ANALYTICAL VS NUMERICAL RESULTS

We perform bifurcation analysis of the LDM [Eq. (10)] using the software MATCONT [68] to understand the origin of the numerically observed solutions of the system (3). First, we take  $K_2 = 8$  and construct the bifurcation diagrams for  $\beta = 1$  and 1.318 by varying  $K_1$ . Figures 3(a) and (b) show the bifurcation diagrams where variations of  $r$  with  $K_1$  have been

presented along with the stability information. For  $\beta = 1$ , the trivial  $r = 0$  solution (solid and dashed black line) becomes unstable via a subcritical pitchfork bifurcation at  $K_1 = 3.6$ . An unstable branch originated from there moves backward (dashed magenta curve) and eventually becomes stable via a saddle-node (SN) bifurcation at  $K_1 = 2.9$ , and move forward (solid magenta curve) as a stable branch. Thus, in the range  $2.9 \leq K_1 \leq 3.6$  bistability is induced which is responsible for the appearance of discontinuous transition for  $\beta = 1$ . Further, on top of the bifurcation diagram, some data points obtained from the numerical simulation (magenta and black circles) are also plotted and a very good agreement is observed. On the other hand, for  $\beta = 1.318$ , the  $r = 0$  branch (solid and black line) becomes unstable via supercritical pitchfork bifurcation at  $K_1 = 8$  and a stable branch is originated (solid green branch) which leads to continuous transition. In this case also, numerical simulation data (green and black circles) closely matches with the analytical ones.

Next, with fixed  $K_1 = 2.5$  we construct two bifurcation diagrams for  $\beta = 0$  and  $0.8$  by varying  $K_2$  [Figs. 3(c) and 3(d)]. For  $\beta = 0$  (solid blue curve), we observe continuous transition and the trivial  $r = 0$  branch (dashed black line) is always unstable in this case. On the other hand, for  $\beta = 0.8$ , zero solution is always stable (solid black line). In addition to that, another pair of non-zero fixed points of the reduced system originated from a SN bifurcation point at  $K_2 = 5.3$ , of which one is stable (solid brown curve) and other one is unstable (dashed brown curve). As a result, bistability occurs for all  $K_2 \geq 5.3$ . Here, the SN bifurcation is responsible for the discontinuous transition to desynchronization. In this case also along with the analytical curve we plot the data obtained from the numerical simulation (brown and black circles) and we observe a very close agreement. It is now apparent that the LDM nicely mimics the dynamics of the whole system. Therefore we proceed for more detailed analysis using the model.

It is important to note here that for fixed  $K_2$  as  $\beta$  is increased starting from 0, the system moves from discontinuous to continuous transition states with the variation of  $K_1$ . The discontinuous transition here is associated with the existence of the SN bifurcation point and it ceased to exist as the SN point meets the trivial ( $r = 0$ ) fixed point. This observation helps to determine the starting point of continuous transition analytically.

The equilibrium points of the LDM [Eq. (10)] are given by  $r = 0$  and

$$r = \sqrt{\frac{K_2 - K_1 \pm \sqrt{(K_1 + K_2)^2 - 8K_2/\cos\beta}}{2K_2}}. \quad (12)$$

Out of two nonzero equilibrium points given in (12), the one obtained with the positive sign (say  $r^+$ ) is stable and the other one (say  $r^-$ ) is unstable in the entire ranges of their existence in the parameter space. Now the SN bifurcation will occur for the parameter values for which  $r^+ = r^-$  and it leads to the relation

$$(K_1 + K_2)^2 \cos\beta = 8K_2 \quad (13)$$

involving the parameters  $K_1$ ,  $K_2$  and  $\beta$ . Thus, for any two given parameters, a feasible solution of the above equation for

the third one will provide the SN bifurcation point. Now when the saddle node point merges with the fixed point  $r = 0$ , the hysteresis will vanish and the system will follow a continuous transition path. Imposing the condition (13) and  $r = 0$  in the equation (12) we can find the point marking the onset of continuous transition, which gives  $K_1 = K_2$ . Using it in the equation (13) the condition for the onset of continuous transition is obtained as

$$K_1 = K_2 = \frac{2}{\cos\beta}. \quad (14)$$

Now in particular, for fixed  $K_2 = 8$ , the onset of continuous transition occurs for  $K_1 = 8$  and  $\beta = \cos^{-1}(1/4) = 1.3181$ . In the numerical simulation, the continuous transition start also occurs exactly at this analytically determined value.

On the other hand, for fixed  $K_1$ , as  $\beta$  is increased, the completely opposite scenario occurs. The trivial fixed point  $r = 0$  is unstable or stable according to  $\beta < \text{or} > \cos^{-1}(\frac{2\Delta}{K_1})$ . In particular, for  $\Delta = 1$  and  $K_1 = 2.5$ ,  $\cos^{-1}(\frac{2\Delta}{K_1}) = 0.6435$ . Thus, for  $\beta < 0.6435$ , the trivial equilibrium point is unstable and it is stable for  $\beta > 0.6435$ . It can be easily checked that for  $\Delta = 1$ ,  $K_1 = 2.5$ , and  $\beta < 0.6435$  only one nontrivial equilibrium point, i.e.,  $r^+$  will exist and be stable. As a result, only continuous transition to synchronization is expected to occur in this parameter regime and it is clearly visible from the numerically obtained blue and bright green curves presented in Fig. 2(b). Whenever  $\beta > 0.6435$ , along with the trivial stable fixed point, both the nontrivial fixed points  $r^+$  and  $r^-$  will exist which marks the existence of bistability leading to discontinuous transition. The analytical result matches very closely with the simulation results presented in Fig. 2(b).

Inspired by the close agreement of the LDM and the numerical simulations results, we use it to construct two parameter diagrams on different projections of the parameter space and present in Fig. 4. Figure 4(a) shows the bifurcations on the  $K_1$ - $\beta$  plane for fixed  $K_2 = 8$ . The magenta curve indicates the backward transition or SN bifurcation points and the black curve indicates the forward transition points [given by Eq. (14)]. The region bounded by these two curves depicts the bistable region. It is observed that the area of bistability reduces with the increase of  $K_1$ . Furthermore, when these two curves meet, the bistability vanishes at the critical point (8,1.318) and the system exhibits synchronization via continuous paths [see Fig. 2(a)] only. At these forward transition points for different lag, the system shows pitchfork bifurcation. When  $\beta$  is greater than (less than) the critical value 1.318, the supercritical (subcritical) pitchfork bifurcation is observed. Here we use the color bar to indicate the values of  $r$  calculated using Eq. (12), considering the stable one. The blue side is for incoherent state; as the color changes from blue to maroon the value of the order parameter  $r$  increases from zero to one. The bistable region is shaded by gray color. Next, on top of the two parameter diagram [Fig. 4(a)], we put the forward (black dots) and backward transition points (magenta dots) obtained from numerical simulations for a comparison. The numerically computed points are found to lie precisely on the analytical curve. These findings demonstrate that the analytical theory correctly captures the system's dynamics.

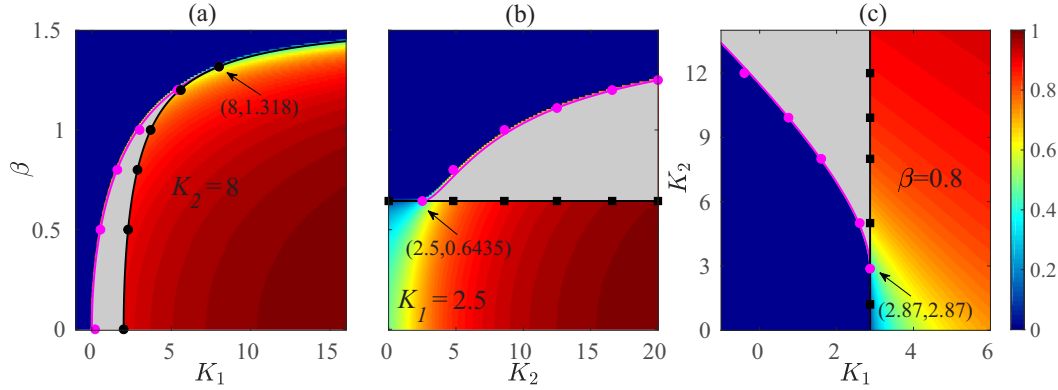


FIG. 4. Two parameter diagrams prepared from the LDM showing the incoherent (blue), coherent (cyan to maroon), and bistable (gray) regimes on the (a)  $K_1$ - $\beta$  plane for  $K_2 = 8$ , (b)  $K_2$ - $\beta$  plane for  $K_1 = 2.5$ , and (c)  $K_1$ - $K_2$  plane for  $\beta = 0.8$ . The color bar represents the synchronization levels measured in terms of  $r$ . The solid magenta curves represent backward transition or SN points. The black curves respectively represent the forward transition points in (a), critical  $\beta$  for the onset of discontinues transition in (b), and forward transition points in (c). The black and magenta dots and squares represent the corresponding points obtained from the numerical simulation.

Moving on to the stability diagram on the  $K_2$ - $\beta$  plane for  $K_1 = 2.5$  [Fig. 4(b)], it is found that the region is divided into three different parts, namely incoherent (blue), coherent (maroon), and bistable (gray). Note that for  $K_1 = 2.5$ , the onset of SN bifurcation point as calculated from the condition (14) takes place at the critical phase - lag  $\beta = 0.643501$  and  $K_2 = 2.5$ . For  $\beta$  less than this critical value, the system follows continuous path and the synchronization level is also high [seen in Fig. 2(b)]. As  $\beta$  is increased a little more, the system exhibits bistability. The numerically computed transition points (magenta dots) shown in the figure show a very close match with the analytical one.

Finally, in Fig. 4(c) we present the stability diagram on the  $K_1$ - $K_2$  plane for  $\beta = 0.8$ . Here the region is also parted into coherent, incoherent, and bistable states as obtained in the previous case. The bistable regime starts at the intersection point of the pitchfork line and the saddle node curve, and the area of this regime broadened with increasing  $K_2$ . From Figs. 4(b) and 4(c) we can conclude that  $K_2$  contributes significantly to promote bistability along with providing a high level of synchronization in the system. It has been verified that for other choices of the fixed values of one of the parameters, similar stability diagrams are obtained. Therefore, in summary, it is observed that  $K_2$  promotes bistability in the system. Moreover, using the results of the LDM, we can appropriately tune the parameters in such a way that  $\beta$  will promote discontinuous transition in the system.

We have also computed the mean-field frequency  $\Omega$  for the phase lag  $\beta = 0.5$ . Figure 5 shows the variations of analytically and numerically obtained  $\Omega$  and  $R$  with the pairwise ( $K_1$ ) and higher order ( $K_2$ ) coupling strengths, respectively. Note that  $\Omega$  ( $= \psi$ ) is analytically calculated from the LDM. In Figs. 5(a) and 5(b) we fix  $K_2$  to 8 and vary  $K_1$ . It is observed that similar to  $r$ ,  $\Omega$  also exhibits explosive transition due to nonlinearity induced by the triadic coupling strength  $K_2$ . Next in Figs. 5(c) and 5(d) we fix  $K_1$  to 2.5 and vary  $K_2$ . In this case both  $r$  and  $\Omega$  exhibit continuous transitions for lower values of phase lag. This figure shows that numerical values (black circles) of both  $r$  and  $\Omega$  closely match with the stable points (red solid line) obtained from the LDM.

V. CONCLUSION

In this paper, the results of our investigation on the effect of phase lag on the transition to synchronization in globally connected networks of phase oscillators in the presence of HOI have been presented.

The numerical simulations with Lorentzian natural frequency reveals two distinct effects of phase - lag: (i) For fixed  $K_2$ , the system exhibits discontinuous transition to synchronization for low  $\beta$  with the variation of  $K_1$ . As  $\beta$  is gradually increased, the system exhibits continuous transition to synchronization when  $\beta$  crosses a critical value. This result is similar to the one observed in the presence of solely pairwise interactions [20,21]. (ii) Surprisingly, the completely opposite scenario is observed in numerical simulations as the higher-order coupling parameter ( $K_2$ ) is varied for a fixed  $K_1$ . For lower  $\beta$ , transition is found to be continuous and the system exhibits discontinuous transition as  $\beta$  is increased

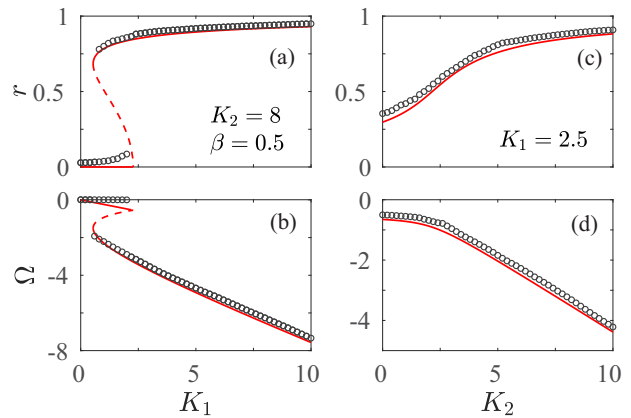


FIG. 5. Order parameter  $r$  and mean-field frequency  $\Omega$  are plotted as a function of [(a)-(b)] pairwise coupling strength  $K_1$  and [(c)-(d)] triadic coupling strength  $K_2$  for phase lag 0.5. The solid and dashed lines (red) are obtained from the LDM, represent stable and unstable fixed points, respectively. The black circles represent the numerically computed points.

beyond a critical value. Therefore, in the presence of HOI, high  $\beta$  promotes discontinuous transition instead of inhibiting it. Simulated results for the mean-field frequency show a similar kind of behavior as  $r$ .

To explain the counter intuitive result mentioned above, a LDM is derived in the thermodynamic limit which faithfully mimic the dynamics of the original system. The bifurcation analysis of the LDM reveals the complex dependence of the transition scenario on the governing parameters. It is observed that the discontinuous transition is always associated with a SN bifurcation. In the first case mentioned above, the SN responsible for discontinuous transition is

associated with a subcritical pitchfork bifurcation, while in the second case, SN bifurcation independently occur in a region of the parameter space. Further, all the analytically derived transition points determined from the LDM show a very good agreement with numerical simulation results.

#### ACKNOWLEDGMENTS

S.D. acknowledges the support from DST, India under the INSPIRE program (Code No. IF190605). C.H. is supported under INSPIRE-Faculty grant (Code No. IFA17-PH193).

- 
- [1] S. Strogatz, *Sync: The Emerging Science of Spontaneous Order* (Penguin UK, 2004).
- [2] A. Pikovsky, M. Rosenblum, J. Kurths, and J. Kurths, *Synchronization: A Universal Concept in Nonlinear Sciences* (Cambridge University Press, 2003).
- [3] Y. Kuramoto, in *Chemical Oscillations, Waves, and Turbulence* (Springer, 1984).
- [4] C.-Q. Wang, A. Pumir, N. B. Garnier, and Z.-H. Liu, *Front. Phys.* **12**, 128901 (2017).
- [5] P. Kumar, D. K. Verma, P. Parmananda, and S. Boccaletti, *Phys. Rev. E* **91**, 062909 (2015).
- [6] U. Lee, M. Kim, K. Lee, C. M. Kaplan, D. J. Clauw, S. Kim, G. A. Mashour, and R. E. Harris, *Sci. Rep.* **8**, 243 (2018).
- [7] B. Blasius and L. Stone, *International Journal of Bifurcation and Chaos* **10**, 2361 (2000).
- [8] J. Pantaleone, *Am. J. Phys.* **70**, 992 (2002).
- [9] J. Grzybowski, E. Macau, and T. Yoneyama, *Chaos: An Interdisciplinary Journal of Nonlinear Science* **26**, 113113 (2016).
- [10] Y. Kuramoto, *Chemical Oscillations, Waves, and Turbulence* (Courier Corporation, 2003).
- [11] J. Buck, *The Quarterly Review of Biology* **63**, 265 (1988).
- [12] S. Yamaguchi, H. Isejima, T. Matsuo, R. Okura, K. Yagita, M. Kobayashi, and H. Okamura, *Science* **302**, 1408 (2003).
- [13] K. Wiesenfeld, P. Colet, and S. H. Strogatz, *Phys. Rev. E* **57**, 1563 (1998).
- [14] F. Dörfler and F. Bullo, *Automatica* **50**, 1539 (2014).
- [15] J. L. van Hemmen and W. F. Wreszinski, *J. Stat. Phys.* **72**, 145 (1993).
- [16] H. Tanaka, A. J. Lichtenberg, and S. Oishi, *Physica D* **100**, 279 (1997).
- [17] D. Pazó, *Phys. Rev. E* **72**, 046211 (2005).
- [18] H. Sakaguchi and Y. Kuramoto, *Prog. Theor. Phys.* **76**, 576 (1986).
- [19] O. E. Omel'chenko and M. Wolfrum, *Phys. Rev. Lett.* **109**, 164101 (2012).
- [20] P. Kundu, P. Khanra, C. Hens, and P. Pal, *Phys. Rev. E* **96**, 052216 (2017).
- [21] P. Kundu and P. Pal, *Chaos: An Interdisciplinary Journal of Nonlinear Science* **29**, 013123 (2019).
- [22] P. Kundu, C. Hens, B. Barzel, and P. Pal, *EPL (Europhysics Letters)* **120**, 40002 (2017).
- [23] M. Brede and A. C. Kalloniatis, *Phys. Rev. E* **93**, 062315 (2016).
- [24] M. Lohe, *Automatica* **54**, 114 (2015).
- [25] L. Q. English, D. Mertens, S. Abdoukary, C. B. Fritz, K. Skowronski, and P. G. Kevrekidis, *Phys. Rev. E* **94**, 062212 (2016).
- [26] M. Lohe, *J. Phys. A: Math. Theor.* **43**, 465301 (2010).
- [27] F. Doörfler and F. Bullo, *SIAM J. Control Optim.* **50**, 1616 (2012).
- [28] E. Omel'chenko and M. Wolfrum, *Physica D* **263**, 74 (2013).
- [29] O. E. Omel'chenko and M. Wolfrum, *Chaos: An Interdisciplinary Journal of Nonlinear Science* **26**, 094806 (2016).
- [30] P. S. Skardal, D. Taylor, J. Sun, and A. Arenas, *Phys. Rev. E* **91**, 010802 (2015).
- [31] P. S. Skardal, D. Taylor, and J. Sun, *Phys. Rev. Lett.* **113**, 144101 (2014).
- [32] P. Khanra, P. Kundu, C. Hens, and P. Pal, *Phys. Rev. E* **98**, 052315 (2018).
- [33] P. Kundu, P. Khanra, C. Hens, and P. Pal, *EPL (Europhysics Letters)* **129**, 30004 (2020).
- [34] P. Khanra and P. Pal, *Chaos, Solitons & Fractals* **143**, 110621 (2021).
- [35] P. Khanra, P. Kundu, P. Pal, P. Ji, and C. Hens, *Chaos: An Interdisciplinary Journal of Nonlinear Science* **30**, 031101 (2020).
- [36] D. Mertens and R. Weaver, *Phys. Rev. E* **83**, 046221 (2011).
- [37] S. Dutta, P. Kundu, P. Khanra, C. Hens, and P. Pal, *Phys. Rev. E* **108**, 024304 (2023).
- [38] S. Adhikari, J. G. Restrepo, and P. S. Skardal, *Chaos: An Interdisciplinary Journal of Nonlinear Science* **33**, 033116 (2023).
- [39] K. Kovalenko, X. Dai, K. Alfaro-Bittner, A. M. Raigorodskii, M. Perc, and S. Boccaletti, *Phys. Rev. Lett.* **127**, 258301 (2021).
- [40] S. Majhi, M. Perc, and D. Ghosh, *J. R. Soc. Interface.* **19**, 20220043 (2022).
- [41] F. Battiston, G. Cencetti, I. Iacopini, V. Latora, M. Lucas, A. Patania, J.-G. Young, and G. Petri, *Phys. Rep.* **874**, 1 (2020).
- [42] U. Alvarez-Rodriguez, F. Battiston, G. F. de Arruda, Y. Moreno, M. Perc, and V. Latora, *Nature Human Behaviour* **5**, 586 (2021).
- [43] I. Iacopini, G. Petri, A. Barrat, and V. Latora, *Nat. Commun.* **10**, 1 (2019).
- [44] L. Martignon, H. Von Hasein, S. Grün, A. Aertsen, and G. Palm, *Biol. Cybern.* **73**, 69 (1995).

- [45] S. Yu, H. Yang, H. Nakahara, G. S. Santos, D. Nikolić, and D. Plenz, *J. Neurosci.* **31**, 17514 (2011).
- [46] C. Giusti, R. Ghrist, and D. S. Bassett, *J. Comput. Neurosci.* **41**, 1 (2016).
- [47] M. W. Reimann, M. Nolte, M. Scolamiero, K. Turner, R. Perin, G. Chindemi, P. Dłotko, R. Levi, K. Hess, and H. Markram, *Front. Comput. Neurosci.* **11**, 48 (2017).
- [48] T. Tanaka and T. Aoyagi, *Phys. Rev. Lett.* **106**, 224101 (2011).
- [49] S. Ghosh, P. Khanra, P. Kundu, P. Ji, D. Ghosh, and C. Hens, *Chaos: An Interdisciplinary Journal of Nonlinear Science* **33**, 053117 (2023).
- [50] P. Jaros, S. Ghosh, D. Dudkowski, S. K. Dana, and T. Kapitaniak, *Phys. Rev. E* **108**, 024215 (2023).
- [51] A. E. Sizemore, C. Giusti, A. Kahn, J. M. Vettel, R. F. Betzel, and D. S. Bassett, *J. Comput. Neurosci.* **44**, 115 (2018).
- [52] S. Chatterjee, S. Nag Chowdhury, D. Ghosh, and C. Hens, *Chaos: An Interdisciplinary Journal of Nonlinear Science* **32**, 103122 (2022).
- [53] J. Grilli, G. Barabás, M. J. Michalska-Smith, and S. Allesina, *Nature (London)* **548**, 210 (2017).
- [54] E. Bairey, E. D. Kelsic, and R. Kishony, *Nat. Commun.* **7**, 1 (2016).
- [55] P. Kareiva, *Ecology* **75** (1994).
- [56] A. Ghasemi and H. Kantz, *Chaos: An Interdisciplinary Journal of Nonlinear Science* **32**, 073101 (2022).
- [57] E. Vasilyeva, A. Kozlov, K. Alfaro-Bittner, D. Musatov, A. Raigorodskii, M. Perc, and S. Boccaletti, *Sci. Rep.* **11**, 5666 (2021).
- [58] V. Salnikov, D. Cassese, and R. Lambiotte, *Eur. J. Phys.* **40**, 014001 (2019).
- [59] A. Costa and M. Farber, in *Configuration Spaces: Geometry, Topology and Representation Theory* (Springer, 2016), pp. 129–153.
- [60] P. S. Skardal and A. Arenas, *Phys. Rev. Lett.* **122**, 248301 (2019).
- [61] C. Xu, X. Wang, and P. S. Skardal, *Phys. Rev. Res.* **2**, 023281 (2020).
- [62] Y. Zhang, V. Latora, and A. E. Motter, *Commun. Phys.* **4**, 195 (2021).
- [63] C. Bick, P. Ashwin, and A. Rodrigues, *Chaos: An Interdisciplinary Journal of Nonlinear Science* **26**, 094814 (2016).
- [64] P. S. Skardal, L. Arola-Fernández, D. Taylor, and A. Arenas, *Phys. Rev. Res.* **3**, 043193 (2021).
- [65] P. S. Skardal and A. Arenas, *Commun. Phys.* **3**, 1 (2020).
- [66] P. Rajwani, A. Suman, and S. Jalan, *arXiv:2302.12076*.
- [67] E. Ott and T. M. Antonsen, *Chaos: An Interdisciplinary Journal of Nonlinear Science* **18**, 037113 (2008).
- [68] A. Dhooge, W. Govaerts, and Y. A. Kuznetsov, *ACM Trans. Math. Softw.* **29**, 141 (2003).